



**HAL**  
open science

## Outlet guide vanes fault detection via vibro-acoustic signal processing

Yasmine Hawwari, Jérôme Antoni, Hugo André, Mohamed El Badaoui

► **To cite this version:**

Yasmine Hawwari, Jérôme Antoni, Hugo André, Mohamed El Badaoui. Outlet guide vanes fault detection via vibro-acoustic signal processing. Forum Acusticum, Dec 2020, Lyon, France. pp.1139-1144, 10.48465/fa.2020.1046 . hal-03235498

**HAL Id: hal-03235498**

**<https://hal.science/hal-03235498>**

Submitted on 27 May 2021

**HAL** is a multi-disciplinary open access archive for the deposit and dissemination of scientific research documents, whether they are published or not. The documents may come from teaching and research institutions in France or abroad, or from public or private research centers.

L'archive ouverte pluridisciplinaire **HAL**, est destinée au dépôt et à la diffusion de documents scientifiques de niveau recherche, publiés ou non, émanant des établissements d'enseignement et de recherche français ou étrangers, des laboratoires publics ou privés.

# OUTLET GUIDE VANES FAULT DETECTION VIA VIBRO-ACOUSTIC SIGNAL PROCESSING

Yasmine Hawwari<sup>1,2</sup> Jérôme Antoni<sup>1</sup> Hugo André<sup>3</sup> Mohamed El Badaoui<sup>2,3</sup>

<sup>1</sup> Laboratoire Vibrations Acoustique, Univ Lyon, INSA-Lyon, F-69621 Villeurbanne, France

<sup>2</sup> SAFRAN TECH, Groupe Safran, 78772 Magny Les Hameaux Cedex, France

<sup>3</sup> 3University of Lyon, UJM-St-Etienne, LASPI, F-42023, Saint-Etienne, France

yasmine.hawwari@insa-lyon.fr

## ABSTRACT

Turbomachinery is subject to several types of fault. The fault diagnosis literature focuses mainly on the mechanical faults related to gearboxes and little interest is given to loss of outlet guide vanes (OGV). This kind of fault causes an efficiency drop in the engine, as the OGV role is to recover the mechanical energy of the induced tangential velocity generated by the fan. Thus, the objective of this study is to design simple and efficient indicators able to detect this fault. This aims at avoiding engine dismounting for visual inspection, especially when it comes to stator of compressor or turbine. The impingement of the fan wake on OGV generates tonal and broadband noise and the noise signature will change with OGV removal. The proposed indicators consider only broadband noise. A healthy reference is to be compared with results of several configurations of OGV loss. Considering that the coupling between the rotor and stator is only acoustical, the emphasis is put on the analysis of acoustic signals. However, considering the structure-borne noise, indicators deduced from vibration signals are also investigated. This approach is applied on vibro-acoustic signals measured on a turbofan and the results of broadband indicator are rather encouraging.

## 1. INTRODUCTION

The rotor alone generates self-noise because of the forces the rotor blades exert on the air and it has both tonal and broadband noise components. The former noise is characterized by the BPF and its harmonics for a subsonic rotor. The broadband noise is mainly due to the trailing edges of the blades. The rotor wake is the sum of a uniform rotating flow plus a turbulent wake from each rotor blade [1]. When a stator is added up to the rotor, the rotor turbulent wakes caused by the boundary layer on the rotor blades i.e. the rotor's trace in the flow downstream of the rotor, will impinge on the stator as depicted in Fig. 1. This creates unsteady pressure fluctuations [2] on the OGV which generates both tonal and broadband noise. The former is caused by the periodicity of the rotor wakes and the stator symmetry and the latter by the turbulence in the wake. In the resultant frequency spectrum, the broadband noise has no dominant frequencies while the tonal noise is char-

acterized by discrete frequencies at blade pass frequency (BPF) and its harmonics as depicted in Fig. 2. Besides, the rotor interacts with other static parts such as the casing and leads to broadband noise generation. This is caused by turbulent boundary layer at the casing wall and occurs because of the small space between the casing and the tips of the rotor blades [3]. After the generation of rotor/stator interaction (RSI) noise, it propagates into the duct through the modal duct transfer functions for tonal and broadband noise. Many researches aim at predicting the rotor/stator interaction (RSI) tonal noise [4], broadband noise [5] and rotor casing interaction noise [6]. The prediction will not be addressed in this paper. For tonal noise, a uniform radial distribution of correlated monopoles located on the stator vane leading edges, is considered. In contrast, for broadband noise, a uniform radial distribution of uncorrelated monopoles located on the stator vanes leading edges, is considered. This leads to the decomposition of the sound field into modes to find out the transmission path into duct. The recorded sound field can be decomposed by applying radial modal decomposition as an inverse method [7]. The sound transmitted into the duct, propagates into the far field and can be calculated at several frequency bins for each mode via the modal energy transmission coefficient, which does not depend on whether it is tonal or broadband noise. More details are given in [8]. However, microphones should be put at discrete locations inside the duct. So if microphones are positioned outside the duct, the radiated field may be scattered and not correspond to the modes propagating into the duct. Thus, in the context of this paper, this approach is not feasible. Radial mode analysis can also be adapted to both tonal and broadband noise components through the consideration of their statistical nature as cyclostationary of order 1 (CS1) and cyclostationary of order 2 (CS2), respectively [9]. It aims to extract the correspondent mode amplitudes from averaged measured sound pressure and the cross-spectral matrix of pressure signals for CS1 and CS2, respectively. Signal decomposition into CS1 and CS2 components can be seen differently by the extraction of the tonal noise with a parametric [10] or non-parametric [11] method and the application of cyclostationarity analysis on the residual signal considered as broadband noise. The study in this paper aims at detecting the OGV loss by considering indicators

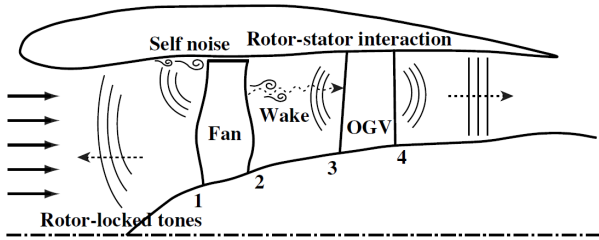


**Figure 1:** Schematic diagram illustrating fan noise sources [12].

based on broadband noise from the analysis of acoustic and vibration signals. This is performed without the extraction of the tonal noise thanks to a robust regression method. Moreover, it is of interest to compare the sensitivity of the transducers according to their position towards the engine.

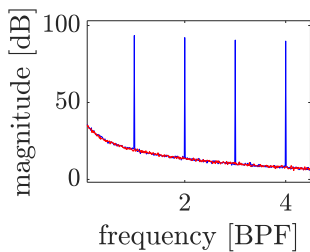


**Figure 2:** Frequency spectrum of the resultant (blue) and broadband (red) noises.

## 2. PROPOSED METHODOLOGY

An intentional OGV fault is created in different configurations in order to investigate the possibility to design indicators based on broadband noise. Comparison between configurations is performed for the same operating regime. The design of simple and efficient indicators to assess OGV loss is targeted. The proposed broadband indicator is based on the characterization of the signal PSD estimate baseline since the more OGVs are removed, the more the flow is turbulent. This means that the background noise is representative of the flow turbulence. In this context, both vibration and acoustic signals will be investigated even though it is already known that this broadband sound is an acoustic source. Let us consider a real-valued time-discrete signal  $\mathbf{x}$  of size  $N$  and PSD  $\mathbf{X}$ . The signal  $\mathbf{x}$  is considered as an addition of two main components  $\mathbf{p}$  and  $\mathbf{r}$ . In the case of the acoustic signal,  $\mathbf{p}$  denotes a deterministic component considered as a sum of sine waves, whereas  $\mathbf{r}$  stands for the effects of flow noise, turbulence and transient events recorded from rotating machinery and has a continuous spectrum without point masses. More explanation of the signal model should be found in [13] for a vibration signal and in [10] for an acoustic signal.  $\mathbf{X}$  can be estimated with the Welch's estimator [14]. It is defined

for signal slices  $x_m(n) = x(n + mR)$  of length  $L$  as:

$$\hat{X}(f) = \frac{1}{MWL} \sum_{m=0}^{M-1} \left| \sum_{n=0}^{L-1} w(n)x_m(n)e^{-j2\pi \frac{f}{f_s}n} \right| \quad (1)$$

where  $R$  is the hop size,  $M$  is the number of available signal slices  $f$  the frequency bins and  $f_s$  is the sampling frequency. The normalizing factor  $W$  denotes the "power" of the temporal window  $w(n)$  expressed as  $W = \frac{1}{L} \sum_{t=0}^{L-1} |w(t)|^2$ .

The idea here is to estimate the PSD of  $\mathbf{r}$  from the baseline of  $\hat{\mathbf{X}}$ . Many ways to extract the baseline can be applied. One way to estimate it, is by calculating the sliding median of the PSD estimate. The median filter adapts quite well to the input signal and eliminates very well the isolated tones influence thanks to its robustness against extreme values. When, the signal length is high, this algorithm may be very time consuming. More details are given in [15]. Moreover, the median filter would give edge effect at the beginning and the end of the signal. In order to alleviate to these drawbacks, the idea is to fit the baseline using robust spline regression [16]. The spline basis can be chosen as the B-spline introduced in [17] as it is suited to computation usage since it is numerically stable. It consists of constructing the B-spline basis  $\mathbf{B}$  of order  $o$  and number of knots  $K$ . These parameters allow to obtain a smoother rendering and adhere to the signal edges. The spline shape depends mainly on choosing  $K$  and their exact locations in order to increase flexibility when the signal trend changes quickly and to avoid overfitting for modest trend changes. This choice is a very complex matter. Thus it was tackled in [18] where an automatic selection of knots was proposed. Then, this basis is used to regress the logarithm of  $\hat{\mathbf{X}}$  through the estimation of the regression vector coefficients. The logarithm transformation of the signal allows homogenizing the signal magnitude and then being robust to peaks. The followed model is written as:

$$\ln \hat{\mathbf{X}} = \mathbf{B}\mathbf{c} + \mathbf{n} \quad (2)$$

where  $\mathbf{c}$  stands for the B-spline coefficients and  $\mathbf{n}$  for i.i.d. noise in a scale-mixture of Gaussians (SMoG). SMoG can be considered as following, for example, Student-t or Generalized Gaussian law. These two distributions were chosen in order to model leptokurtic noises since the baseline to be estimated is submerged with peaks. Then, the idea is to find the function coefficients  $\mathbf{c}_{\min}$  fitting the data by minimizing a certain cost function based on  $\mathbf{n}$  PDF. The estimation is performed recursively until the maximum number of iterations or a very tight difference between the previous the recent and previous regression vector, is attained. The estimated baseline  $\mathbf{Y}$  is obtained as:

$$\mathbf{Y} = \exp(\mathbf{B}\mathbf{c}_{\min}) \quad (3)$$

After the estimation of  $\mathbf{Y}$ , it is necessary to design a scalar indicator sensitive to OGV removal and allowing the comparison between the transducers sensitivity to this fault. In this study, only the mean value of the baseline at each configuration and several transducers will be retained as a

scalar broadband noise indicator. It is worthy to recall that the broadband noise indicator should be compared with observations acquired in the same operating conditions because if, for example, the air intake causes more turbulence in contact with the rotor blades, this arises as more broadband noise. The same goes for conditions such as the sweep and lean angles of stator.

### 3. EXPERIMENTAL SETUP

#### 3.1 Bench presentation

DGEN380 is the world’s smallest turbofan (a double flow engine) which is completely developed and tested by Price Induction. It was acquired by the engineering school ISAE-SUPAERO. This kind of engine is more and more used because of their higher efficiency with respect to one flow engines. First, the air is ingested by the fan and after splitting it into two streams, the first stream air is compressed through the compressor, mixed with the fuel, burnt in the combustion chamber and expanded through the turbine. This cycle is called the Brayton thermodynamic cycle. Then, the turbine rotates the fan and the compressor. For the second stream air, it is straightened through the OGVs and accelerated through the nozzle. A descriptive scheme is given in Fig. 3.

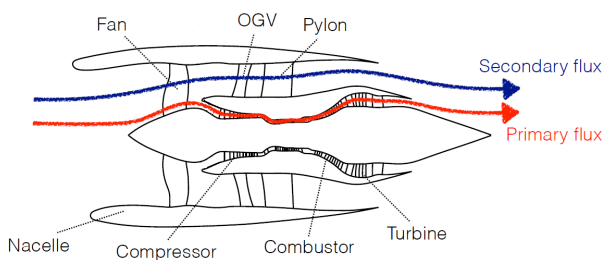


Figure 3: Turbofan engine scheme adapted from [19].

#### 3.2 acquisition system

The acquisition was performed on DGEN 380 put in a reverberation chamber. The bench is instrumented with intrusive measurements such as 3-axis accelerometers of reference A/34-2 placed all along the engine at positions 2A, 2RU and 22A for accelerometer 1, 2 and 3, respectively as illustrated in Fig. 4(a). The  $x_{axis}$  is parallel to the flow direction while y and z axes are perpendicular to the latter. Non-intrusive measurements are based on 11 identical free-field 0° incidence microphones of reference 40PH of 1/4” (G.R.A.S). They were placed all around the engine as depicted in Fig. 4(b). These transducers are connected to the acquisition central to yield digital signals at  $f_s = 40.96$  kHz and on a time duration of 40s ( $N = 1654784$ ).

#### 3.3 measurement campaign

As previously evoked, the only artificial fault is the progressive OGV removal. The fault was created under bloc removal configurations. According to expert opinions, the

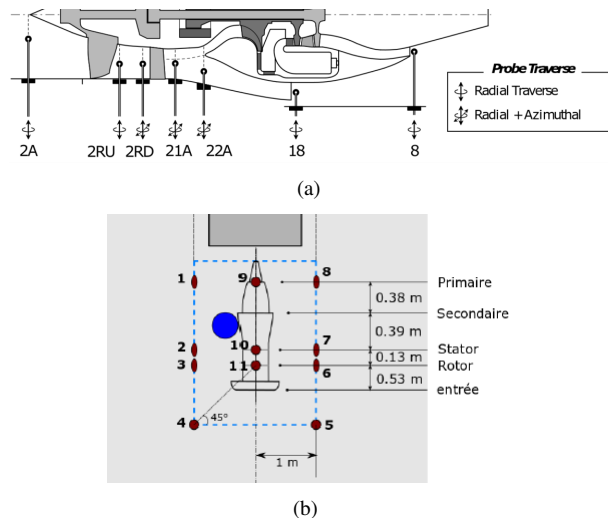


Figure 4: Positions of the accelerometers (a) and microphones (b).

OGV loss by bloc is the more likely to happen since when one OGV is lost, the neighbor OGVs are directly affected. These configurations are depicted in Fig. 5. The turbofan operates at constant regimes called the stepwise operating mode. It is repeated 10 times for 9 speed steps taking discreet values of fan rotation in an ascendant variation from speed ‘1’ (800 rpm) passing by speed ‘2’ (4400 rpm), speed ‘3’ (6900 rpm) and speed ‘4’ (9400 rpm) until speed ‘5’ (12000 rpm) and then descendant variation from 12000 rpm to 800 rpm. Since the ascendant and descendant parts are symmetric, only the ascendant part will be considered in this study. Moreover, speed1 corresponds to ventilation regime (i.e. the engine startup). Therefore, it will be omitted in the following application in order to avoid unstable results.

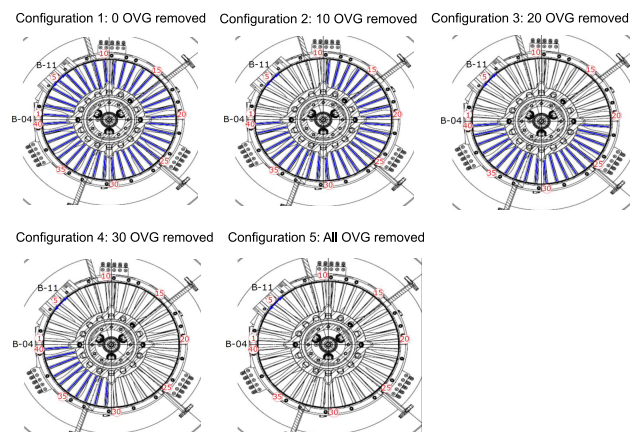


Figure 5: OGV removal configurations.

### 4. EXPERIMENTAL RESULTS AND DISCUSSION

In order to compute the proposed broadband noise indicator, the Welch’s PSD estimate ( $L = f_s/2$ ,  $R = L/2$ ) of vibration and acoustic signals for each OGV configuration WRT to the 10 runs and the four operating speeds,

are obtained. An example of the Welch's PSD estimate of vibration and acoustic signals at speed '2' (speed '5') from one run, are depicted in Fig. 6 (Fig. 7). Fig. 6(a), 6(b), 6(c) and 6(d) refer to microphone 5 (engine inlet), microphone 8 (engine outlet), accelerometer 1  $x_{axis}$  (fan upstream in the flow direction), and accelerometer 3  $x_{axis}$  (stator downstream in the flow direction), respectively. The same is considered for Fig. 7. Then, the baseline of each PSD estimate is obtained through the application of the B-spline regression of  $o = 3$  and  $K = 34$ . The baselines correspondent to the Welch's PSD estimates of Fig. 6 and Fig. 7 for 10 runs are depicted in Fig. 8 and Fig. 9, respectively.

#### 4.1 Acoustic signals

The obtained baselines from acoustic signals showed that the more the OGVs are removed the more, the baseline is elevated which means an increase of broadband noise. This is particularly emphasized at full speed (speed '5') where the discrepancy between configuration 1 and configuration 5 is considerable. It is also noticeable that this noise propagates from the fan inlet (Fig. 8(a), Fig. 9(a)) to the outlet (Fig. 8(b), Fig. 9(b)) into the duct. This is valid for all the considered configurations and speed regimes. This is explained by the increasing turbulent character of the flow with the OGV removal as it is less oriented. This reflects directly on the broadband noise content since it is caused by turbulence. Then, the proposed scalar indicators from the obtained baselines are calculated and presented in Fig. 10 (left). Fig. 10(a), 10(c), 10(e) and 10(g) correspond to speed '2', '3', '4' and '5', respectively. In each of the latter subfigures, each curve correspond to one microphone and each point of the same curve correspond to the average of the indicators obtained from 10 runs for the same OGV configuration. Only the microphones 5, 6, 7, 8, 9, 10, 11 are represented to avoid redundancy because of the symmetric layout of the microphones. The results from acoustic signals show a monotonous trend for all speed regimes. This monotonous trend is showed for all the microphones regardless of their positions.

The proposed broadband noise indicator seems very reliable for OGV loss detection. It is worthy to note that all the scalar indicators were uniformly normalized by their maximum value for each transducer in order to enhance the readability of the indicators. After a closer look to the indicators from acoustic signals, it is noticeable that indicators from upstream and downstream the fan are more sensitive to broadband noise than those from downstream the stator downstream. This is explained by the fact that the broadband noise can propagate upstream and downstream the fan which means that if a part from the broadband noise propagates upstream the fan, only the residue will appear downstream the stator. Moreover, the broadband noise propagating through the engine is distorted by the mean flow and undergoes diffraction and reflection by the blades of the several component [20]. This may weaken the broadband noise seen downstream the stator. Last, the broadband noise transmitted to the far field out of the tur-

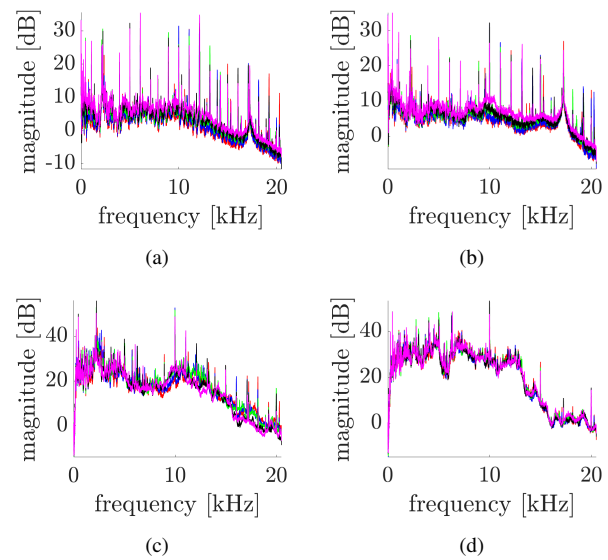


**Figure 6:** Welch's PSD estimate of signals (1 run) from microphone 5 (a), microphone 8 (b), accelerometer 1 ( $x_{axis}$ ) (c) and accelerometer 3 ( $x_{axis}$ ) (d) at speed '2': configuration 1 (red), configuration 2 (blue), configuration 3 (green), configuration 4 (black) and configuration 5 (magenta).

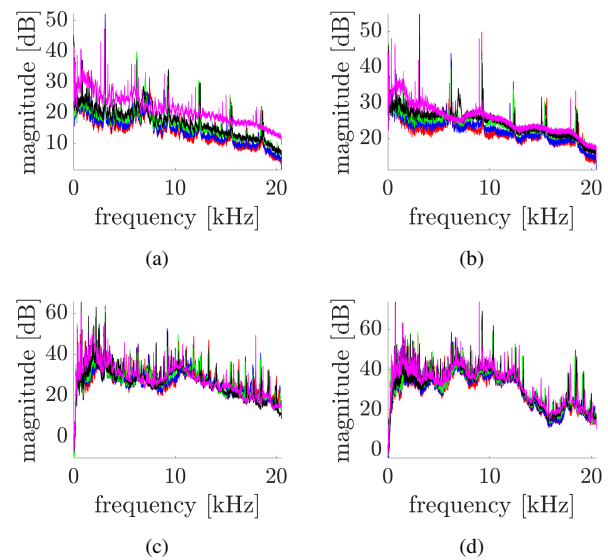


**Figure 7:** Welch's PSD estimate of signals (1 run) from microphone 5 (a), microphone 8 (b), accelerometer 1 ( $x_{axis}$ ) (c) and accelerometer 3 ( $x_{axis}$ ) (d) at speed '5': configuration 1 (red), configuration 2 (blue), configuration 3 (green), configuration 4 (black) and configuration 5 (magenta).

bofan is further weakened (microphones 8 and 9).

#### 4.2 Vibration signals

Even though the turbulence can be intuitively considered as propagating via airborne to create the broadband acoustic noise, it is also propagating via structure-borne and gener-

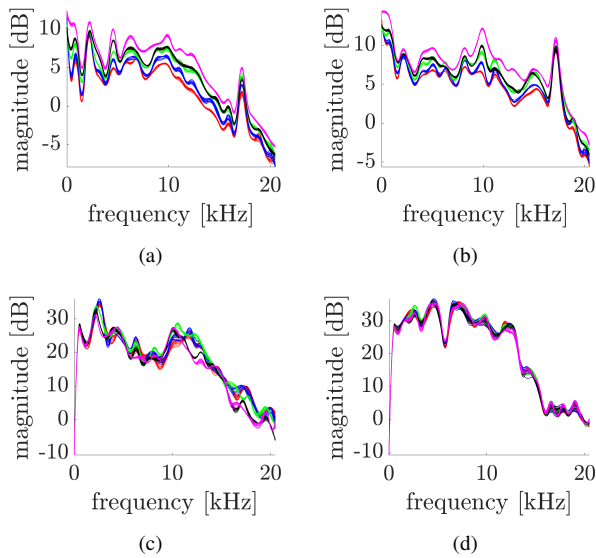


**Figure 8:** The estimated baselines of signals (10 runs) from microphone 5 (a), microphone 8 (b), accelerometer 1 ( $x_{axis}$ ) (c) and accelerometer 3 ( $x_{axis}$ ) (d) at speed ‘2’: configuration 1 (red), configuration 2 (blue), configuration 3 (green), configuration 4 (black) and configuration 5 (magenta).

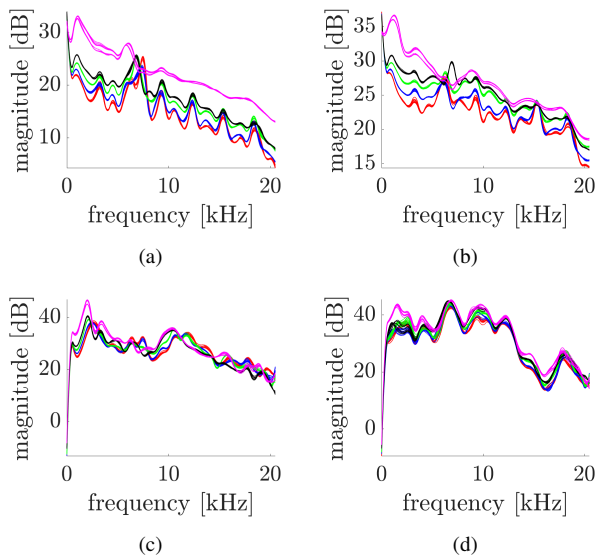


**Figure 9:** The estimated baselines of signals (10 runs) from microphone 5 (a), microphone 8 (b), accelerometer 1 ( $x_{axis}$ ) (c) and accelerometer 3 ( $x_{axis}$ ) (d) at speed ‘5’: configuration 1 (red), configuration 2 (blue), configuration 3 (green), configuration 4 (black) and configuration 5 (magenta).

ates the casing vibrations. Note also that this second propagation path can be transformed again to airborne but it would have less contribution in comparison with the direct airborne path. Thus the same characterization of turbulence was applied to vibration signals. On the opposite of the baselines (Fig. 8 and Fig. 9) obtained from the acoustic signals, those obtained from vibration signals show less

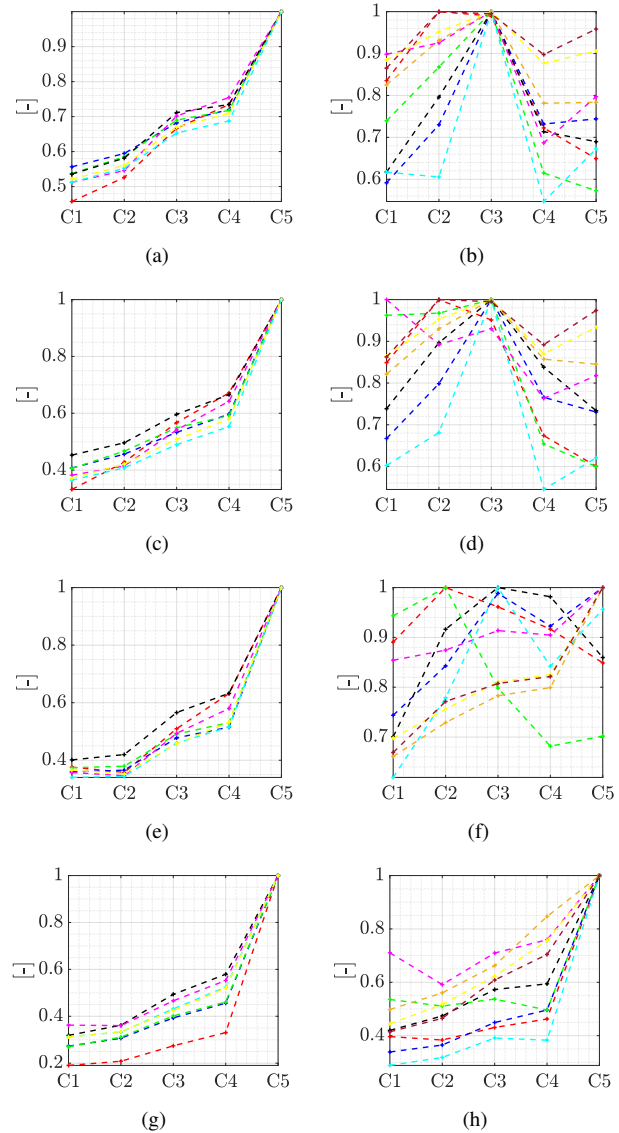


**Figure 10:** Broadband noise scalar indicators averaged on 10 runs from acoustic signals (left) vibrations signals (right), respectively WRT OGV configurations (‘C1’, ‘C2’, ‘C3’, ‘C4’ and ‘C5’ correspond to configuration 1, 2, 3, 4 and 5, respectively): (a)(b) speed ‘2’, (c)(d) speed ‘3’, (e)(f) speed ‘4’ and (g)(h) speed ‘5’. Microphones: 5 (red), 6 (blue), 7 (green), 8 (black), 9 (magenta), 10 (cyan), 11 (yellow). Accelerometers: 1 ( $x_{axis}$  (red),  $y_{axis}$  (blue),  $z_{axis}$  (green)), 2 ( $x_{axis}$  (black),  $y_{axis}$  (magenta),  $z_{axis}$  (cyan)), 3 ( $x_{axis}$  (yellow),  $y_{axis}$  (mustard),  $z_{axis}$  (brown)).

separability especially for low speed regimes. The baselines depicted in the latter figures correspond to the fan upstream and the stator downstream (in the flow direction). Similarly to acoustic signals, the indicators for vibration signals are calculated for the three accelerometers (3 axes) corresponding to the fan downstream and upstream as well as the stator downstream (Fig. 10 (right)). Regarding the obtained indicators, it was observed that the sensitivity to broadband noise was only observed at full speed for upstream the fan and downstream the stator. This was noticed because at full speed, the generated broadband noise

is sufficiently strong to generate noticeable variation of the structure vibrations. Thus, the indicators deduced from vibration signals are not reliable. Therefore, the proposed broadband indicator will be only considered for acoustic signals.

### 4.3 Conclusion

In this paper a solution to detect OGV loss faults from vibro-acoustic signals, regarding broadband noise, was proposed. It was shown that the deduced indicators from acoustic signals were very reliable while those deduced from vibration signals were not retained since they were sensitive only in high speed regime conditions. In a further work, an indicator based on tonal noise should be proposed. Later on, it would be interesting to explore other types of faults on the test bench such as pitting and cracking faults and/or acquire observations on long time duration in order to investigate fatigue. Last, it is suited to apply an algorithm of parametric normalization towards, for instance, speed, temperature and pressure conditions in order to obtain normalized indicators WRT operating conditions.

## 5. REFERENCES

- [1] J. R. Mathews, *Mathematical modelling of noise generation in turbofan aeroengines using Green's functions*. PhD thesis, Department of Applied Mathematics and Theoretical Physics, University of . . . , 2016.
- [2] J. B. H. M. Schulten, "Sound generation by ducted fans and propellers as a lifting surface problem.," 1994.
- [3] N. Peake and A. B. Parry, "Modern challenges facing turbomachinery aeroacoustics," *Annual Review of Fluid Mechanics*, vol. 44, pp. 227–248, 2012.
- [4] D. Nark, E. Envia, and C. Burley, "On acoustic source specification for rotor-stator interaction noise prediction," in *16th AIAA/CEAS Aeroacoustics Conference*, p. 3713, 2010.
- [5] H. Posson, S. Moreau, and M. Roger, "Broadband noise prediction of fan outlet guide vane using a cascade response function," *Journal of Sound and Vibration*, vol. 330, no. 25, pp. 6153–6183, 2011.
- [6] M. B. Meingast, A. Batailly, M. Legrand, and J.-P. Ousty, "Investigation of rotor-casing interactions in the centrifugal compressor of a helicopter engine," in *Turbo Expo: Power for Land, Sea, and Air*, vol. 55270, p. V07BT31A009, American Society of Mechanical Engineers, 2013.
- [7] E.-E. Ioannou, "Singular value decomposition (svd) for the optimization of microphone measurement positions for sound propagation studies," *Diploma thesis*, 2013.
- [8] A. Moreau and L. Enghardt, "Improvements of a parametric model for fan broadband and tonal noise," *Journal of the Acoustical Society of America*, vol. 123, no. 5, p. 3540, 2008.
- [9] M. Behn, B. Pardowitz, and U. Tapken, "Separation of tonal and broadband noise components by cyclostationary analysis of the modal sound field in a low-speed fan test rig," in *International Conference of Fan Noise, Aerodynamics, Applications and Systems*, pp. 18–20, 2018.
- [10] D. B. Stephens and H. Vold, "Order tracking signal processing for open rotor acoustics," *Journal of Sound and Vibration*, vol. 333, no. 16, pp. 3818–3830, 2014.
- [11] D. Gabor, "Theory of communication. part 1: The analysis of information," *Journal of the Institution of Electrical Engineers-Part III: Radio and Communication Engineering*, vol. 93, no. 26, pp. 429–441, 1946.
- [12] T. Suzuki, P. R. Spalart, M. L. Shur, M. K. Strelets, and A. K. Travin, "Unsteady simulations of a fan/outlet-guide-vane system: Tone-noise computation," *AIAA Journal*, vol. 56, no. 9, pp. 3558–3569, 2018.
- [13] H. Wold, *A study in the analysis of stationary time series*. PhD thesis, Almqvist & Wiksell, 1938.
- [14] P. Welch, "The use of fast fourier transform for the estimation of power spectra: a method based on time averaging over short, modified periodograms," *IEEE Transactions on audio and electroacoustics*, vol. 15, no. 2, pp. 70–73, 1967.
- [15] M. Durnerin, *Une stratégie pour l'interprétation en analyse spectrale. Détection et caractérisation des composantes d'un spectre*. PhD thesis, Institut National Polytechnique de Grenoble-INPG, 1999.
- [16] J. Antoni, Q. Leclere, and E. Julliard, "Extraction des composantes aéroacoustiques tonales et larges bandes," *14ème Congrès Français d'Acoustique: CFA*, 2018.
- [17] B. De and D. BOOR, "A practical guide to splines," 1978.
- [18] V. Goepp, O. Bouaziz, and G. Nuel, "Spline regression with automatic knot selection," *arXiv preprint arXiv:1808.01770*, 2018.
- [19] M. Daroukh, *Effects of distortion on modern turbofan tonal noise*. PhD thesis, 2017.
- [20] M. Leyko, *Mise en oeuvre et analyse de calculs aéroacoustiques de type SGE pour la prévision du bruit de chambres de combustion aéronautiques*. PhD thesis, Toulouse, INPT, 2010.